Convectively coupled wave–environment interactions

SAMUEL N. STECHMANN[12]†, ANDREW J. MAJDA[3] AND DMITRI SKJORSHAMMER[4]

[1]Department of Mathematics, and Department of Atmospheric and Oceanic Sciences, University of California, Los Angeles, Los Angeles, CA 90095, USA

[2]Department of Mathematics, University of Wisconsin–Madison, Madison, WI 53706, USA

[3]Department of Mathematics, and Center for Atmosphere–Ocean Science, Courant Institute, New York University, New York, NY 10012, USA

[4]Department of Mathematics, Harvey Mudd College, Claremont, CA 91711, USA

(Received this version: June 22, 2011)

In the tropical atmosphere, waves can couple with water vapor and convection to form large-scale coherent structures called convectively coupled waves (CCW). The effects of water vapor and convection lead to CCW–mean flow interactions that are different from traditional wave–mean flow interactions in many ways. CCW–mean flow interactions are studied here in two types of models: a multiscale model that represents CCW structures in two spatial dimensions directly above the Earth's equator, and an amplitude model in the form of ordinary differential equations for the CCW and mean flow amplitudes. The amplitude equations are shown to capture the qualitative behavior of the spatially resolved model, including nonlinear oscillations and a Hopf bifurcation as the climatological background wind is varied. Furthermore, an even simpler set of amplitude equations can also capture some of the essential oscillatory behavior, and it is shown to be equivalent to the Duffing oscillator. The basic interaction mechanisms are that the mean flow's vertical shear determines the preferred propagation direction of the CCW, and the CCWs can drive changes in the mean shear through convective momentum transport, with energy transfer that is sometimes upscale and sometimes downscale. In addition to CCW–mean flow interactions, also discussed are CCW–water vapor interactions, which form the basis of the Madden–Julian Oscillation (MJO) skeleton model of the first two authors. The key parameter of the MJO skeleton model is estimated theoretically and is in agreement with previously conjectured values.

1. Introduction

Wave interactions and wave–mean flow interactions have a long history in fluid dynamics and in atmospheric fluid dynamics in particular (Plumb 1977; Andrews & McIntyre 1978; Craik 1985; Baldwin *et al.* 2001; Bühler 2009). In the atmosphere, the traditional setting for wave–mean flow interactions is in the stratosphere. In this paper, by contrast, we consider waves in the different setting of the troposphere, in the tropics, where the waves can couple with water vapor and convection to form large-scale coherent structures called convectively coupled waves (CCW), among many types of propagating convective features. Furthermore, in this setting, it is not only the mean flow that is important but also the mean moist thermodyanamic state. Hence, this is a setting for convectively

† Email address for correspondence: stechmann@wisc.edu

coupled wave–environment interactions, among a wide variety of interactions between convection, waves, and their background environment.

In the tropical troposphere, clouds and convection are organized across many different scales, and the largest scales can be loosely partitioned into three groups. Individual cloud systems appear on scales of roughly 200 km and 0.5 days, and they are commonly called "mesoscale convective systems" (MCS) (Houze 2004). Several MCS, in turn, can sometimes be organized within a larger-scale wave envelope with scales of roughly 2000 km and 5 days; these propagating envelopes are called CCW (Kiladis *et al.* 2009), and their structure is illustrated schematically in figure 1. Moreover, several CCW can sometimes be organized within an even larger-scale wave envelope with scales of roughly 20 000 km and 50 days; the most prominent example of this is the Madden–Julian Oscillation (MJO) (Lau & Waliser 2005; Zhang 2005).

Many aspects of MCS and MCS–environment interactions have been studied previously. It is well-known that MCS can affect the larger-scale fields of momentum, temperature, and moisture in which they exist (Yanai *et al.* 1973; LeMone 1983; Houze 1989; LeMone & Moncrieff 1994), and the energy transfers are sometimes upscale and sometimes downscale. It is also well-known that the larger-scale environment influences the MCS that form within it (Moncrieff & Green 1972; Barnes & Sieckman 1984; LeMone *et al.* 1998). Nevertheless, many details of MCS–environment interactions are still being studied (Johnson *et al.* 2005). A complex form of MCS–environment interactions is the way in which many MCS become grouped together to form a CCW (Nakazawa 1988; Mapes 1993; Grabowski & Moncrieff 2001; Khouider & Majda 2006; Stechmann & Majda 2009; Tulich *et al.* 2007). As illustrated schematically in figure 1, many processes are believed to play a role, including interactions of convection, gravity waves, wind shear, and moist thermodynamics.

On larger scales, CCW are arguably more recently observed and less understood than MCS. CCW properties have been identified in several observational studies (Takayabu 1994*a*,*b*; Wheeler & Kiladis 1999; Wheeler *et al.* 2000; Kiladis *et al.* 2009), but CCW–environment interactions have been studied very little, although some studies have analyzed observations of CCW in different seasons or hemispheres (Wheeler & Kiladis 1999; Roundy & Frank 2004; Yang *et al.* 2007). A complex form of CCW–environment interactions is the way in which CCW interact with larger-scale structures such as the MJO, in which the CCW are often embedded.

In fact, one important motivation for understanding CCW–environment interactions is for better understanding the MJO, which is a planetary-scale envelope of sub-planetary-scale convection including CCW (Nakazawa 1988; Hendon & Liebmann 1994; Dunkerton & Crum 1995). Despite the importance of the MJO, computer general circulation models (GCMs) typically have poor representations of it (Lin *et al.* 2006; Kim *et al.* 2009), and there is still no generally accepted theory for its fundamental physical mechanisms. Nevertheless, some recent non-traditional GCM approaches appear to capture many of the observed features of the MJO by accounting for the smaller-scale convective features within the MJO envelope (Benedict & Randall 2009; Khouider *et al.* 2011*b*). In addition, Majda & Stechmann (2009*b*, 2011) recently introduced a minimal model for the MJO's "skeleton" in which CCW–water vapor interactions are part of the proposed fundamental mechanism, and the model recovers the key features of the observed MJO skeleton. Furthermore, CCW–mean flow interactions appear to account for additional features of the MJO – its "muscle" – beyond the features of its "skeleton" (Majda & Biello 2004; Biello & Majda 2005; Majda & Stechmann 2009*a*), and the energy transfer from convective momentum transport (CMT) is sometimes upscale and sometimes downscale.

One purpose of the present paper is to further study the CCW–mean flow interactions

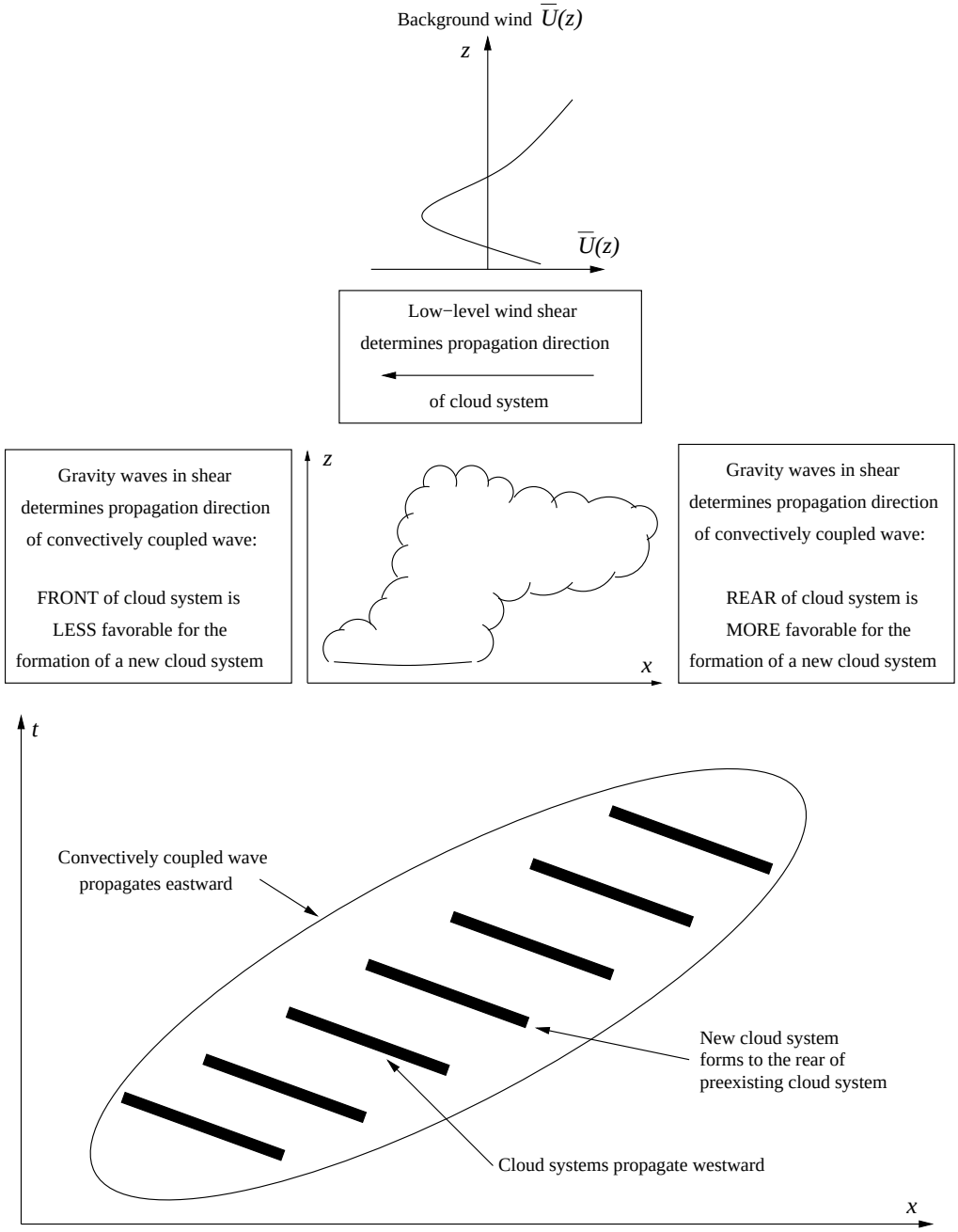

FIGURE 1. Schematic diagram of a convectively coupled wave and the cloud systems embedded within it. Anvil-shaped cloud systems propagate eastward or westward depending on the low-level vertical shear in the background wind (LeMone *et al.* 1998), and new cloud systems form repeatedly on one preferred side of preexisting cloud systems (Nakazawa 1988; Grabowski & Moncrieff 2001; Tulich *et al.* 2007), with the preferred side determined by the background shear (Stechmann & Majda 2009). The result is a propagating wave train of cloud systems.

of Majda & Stechmann (2009*a*), including using amplitude equations as a simplified ordinary differential equation (ODE) model for the interactions, as has been done in other fluid dynamics settings (Craik 1985; Guckenheimer & Mahalov 1992; Bourlioux & Majda 1995; Ruzmaikin *et al.* 2003). The dynamics of the CCW–mean flow interactions of Majda & Stechmann (2009*a*) include interesting nonlinear oscillations and a Hopf bifurcation, and it will be shown that simple amplitude ODEs can capture this dynamical behavior. While a systematic asymptotic derivation of the amplitude ODEs is not given (due to the complicated form of the nonlinearities in the governing equations), the form of the amplitude ODEs are motivated by systematic derivations in other scientific settings (Bourlioux & Majda 1995). In addition to CCW–mean flow interactions, a second purpose of the present paper is to investigate CCW–water vapor interactions, which serves to further justify the use of an amplitude equation in the MJO skeleton model of Majda & Stechmann (2009*b*, 2011), beyond the phenomenological motivation given previously, and to provide a theoretical estimate for the key parameter of the model.

The paper is organized as follows. In section 2 the focus is CCW–mean flow interaction, and in section 3 it is CCW–water vapor interaction. Section 4 provides a concluding discussion.

2. CCW–mean flow interactions

As described above, momentum interactions are often studied as part of either wave–environment or convection–environment interaction, as either wave–mean flow interactions or convective momentum transport. The topic of CCW–mean flow interactions involves some aspects of both. In subsections 2.1–2.3, we study the effect of the mean flow on CCWs, the effect of CCWs on the mean flow, and finally the two-way interactions between CCWs and the mean flow.

2.1. *Effect of mean flow on CCW*

To investigate CCW dynamics, we use the multicloud model of Khouider & Majda (2006, 2008), which is a spatially variable partial differential equation (PDE) model for CCWs that captures many important features such as their propagation speeds and tilted vertical structures. The mathematical form of the model is

$$\partial_t \boldsymbol{u} + \mathsf{A}(\boldsymbol{u})\partial_x \boldsymbol{u} = \boldsymbol{S}(\boldsymbol{u}) \tag{2.1}$$

where $\boldsymbol{u}(x,t)$ is a vector of model variables, $\boldsymbol{u} = (u_1, \theta_1, u_2, \theta_2, \theta_{eb}, q, H_s)^T$. The model variables are u_j, the zonal velocity in the jth baroclinic mode; θ_j, the potential temperature in the jth baroclinic mode; θ_{eb}, the equivalent potential temperature of the boundary layer; q, the vertically integrated water vapor; and H_s, the stratiform heating rate. The matrix $\mathsf{A}(\boldsymbol{u})$ includes the effects of nonlinear advection and pressure gradients, and $\boldsymbol{S}(\boldsymbol{u})$ is a nonlinear interactive source term with combinations of polynomial nonlinearities and nonlinear switches. The detailed form of these equations is shown in the appendix.

Using the velocity modes $u_j(x,t)$, the two-dimensional zonal velocity $u(x,z,t)$ is recovered as a sum of the contributions from all of the vertical modes:

$$u(x,z,t) = u_0(x,t) + \sum_{j=1}^{\infty} u_j(x,t)\ \sqrt{2}\cos(jz) \tag{2.2}$$

where the troposphere extends from $z = 0$ to π in the nondimensional units shown in (2.2), which corresponds to $z = 0$ to 16 km in dimensional units. The vertically uniform

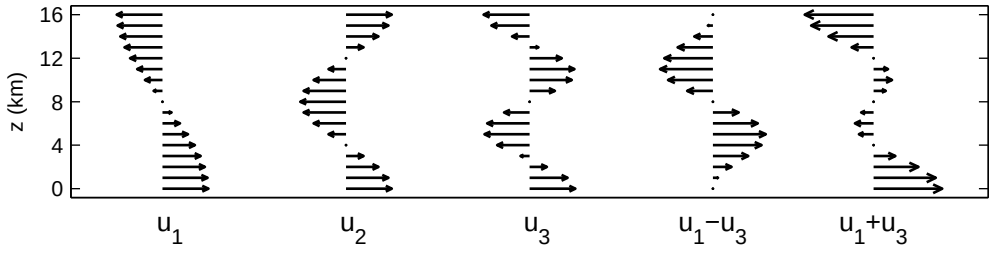

FIGURE 2. Vertical structures of different baroclinic modes and baroclinic mode combinations.

mode $j = 0$ is the barotropic mode, and the other modes are the baroclinic modes. Plots of the vertical structure associated with some of the vertical baroclinic modes are shown in figure 2. In order to include a balance between simplicity and important physical effects, the original multicloud model includes only u_1 and u_2 as dynamical variables. The effect of u_3 will also be considered here as either a constant background shear $\bar{U}_3$ or as a slowly evolving mean shear $\bar{U}_3(T)$, where $T = \epsilon^2 t$ is a slow time scale.

Figure 3 shows the behavior of the multicloud model (2.1) in the presence of three different mean shears $\bar{U}(z)$. These are nonlinear simulations on a 6000-km-wide domain with periodic boundary conditions in the horizontal. The first column shows the case of zero mean shear. In this case, there are linear instabilities over a finite band of wavenumbers, the unstable waves propagate both eastward and westward, and there is perfect east–west symmetry. In the nonlinear simulation, a westward-propagating traveling wave arises as the stationary solution (if viewed from a translating reference frame), which grows from a small initial random perturbation. Due to the perfect east–west symmetry of this case, the initial conditions randomly select whether the eastward- or westward-propagating wave will eventually become the stationary solution. The second column shows a case with a lower tropospheric westerly jet and an upper tropospheric easterly jet. In this case, the east–west symmetry is broken, the westward-propagating wave has the largest linear theory growth rates, and it is the eventual stationary solution in the nonlinear simulation. The third column shows another case with a nontrivial vertical shear. In this case, the linear theory growth rates are nearly east–west symmetric, and the nonlinear simulation appears to favor a standing wave solution rather than a travelling wave solution. In fact, at later times (not shown), there is an oscillation between the standing and travelling wave states in this case, so the preference for the standing wave is tenuous. [It is possible that a different parameter regime of the multicloud model may show a more robust standing wave state, but the present parameter regime is chosen to match that of Majda & Stechmann (2009*a*).] Nevertheless, these cases demonstrate, to an extent, two effects of the background shear on the CCWs: it can break the east–west symmetry to favor either the eastward- or westward-propagating wave, and it can determine, to an extent, whether a traveling wave or standing wave state is favored.

The competition between the traveling wave and standing wave states also appears in other scientific contexts such as combustion (see Bourlioux & Majda (1995) and references therein). In these other contexts, a useful tool for understanding this competition has been wave amplitude equations, which can sometimes be derived from the governing equations using systematic asymptotics. Here, since the multicloud model of (2.1) includes complicated combinations of polynomial nonlinearities and nonlinear switches, we use amplitude equations as a qualitative model without carrying out a systematic asymptotic derivation for them. The end results will suggest that amplitude equations can capture the basic dynamical behavior of the multicloud model.

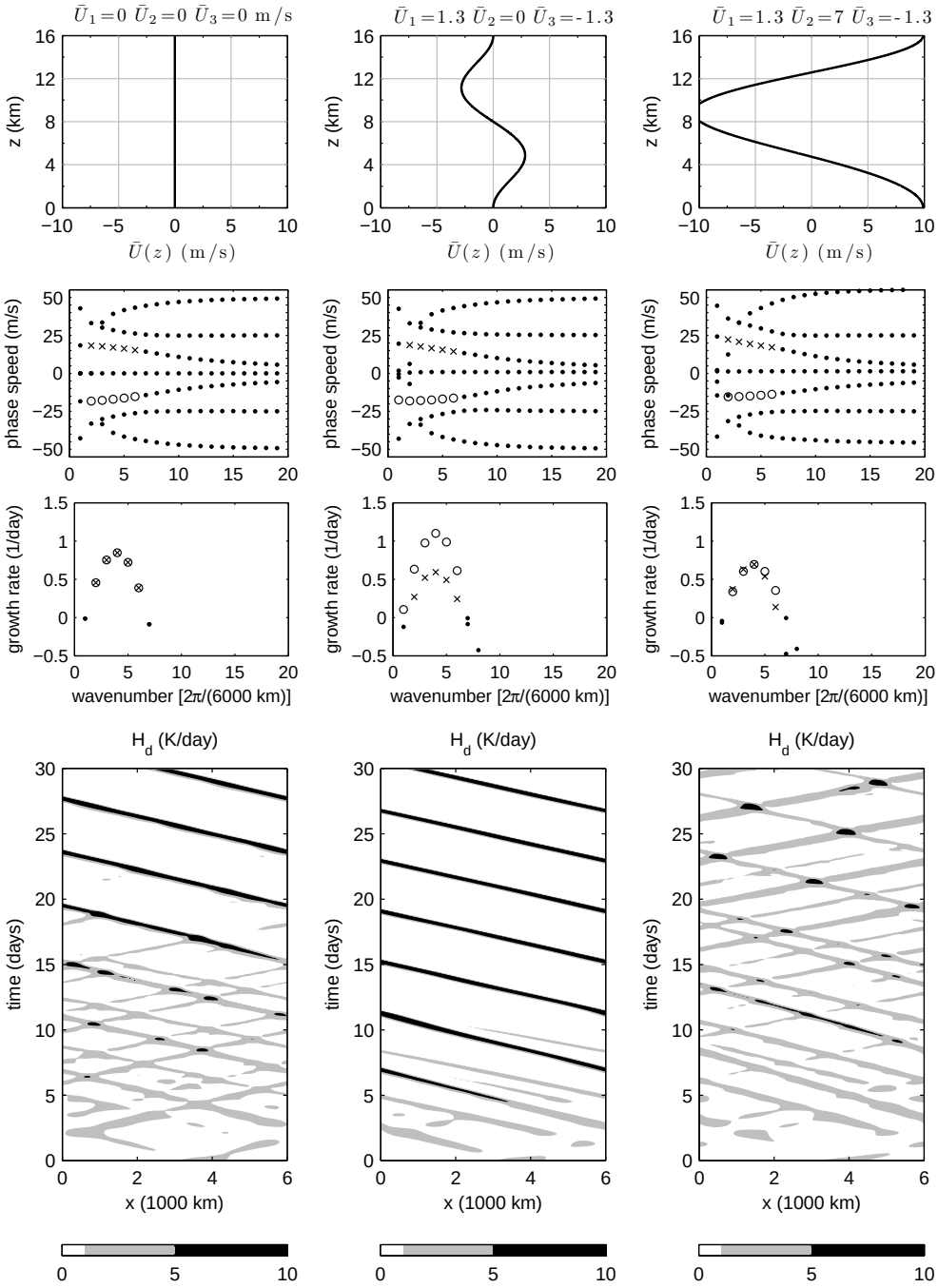

FIGURE 3. Linear theory and nonlinear simulations for three cases of fixed background shear. Row 1: Three different mean flows $\bar{U}(z)$ used for the three cases. Row 2: Phase speed as a function of wavenumber for the linear modes. Row 3: Growth rate as a function of wavenumber for the linear modes. Filled circles denote damped modes, and crosses and open circles denote eastward- and westward-propagating unstable modes, respectively. Row 4: Space–time plots of deep convective heating $H_d(x,t)$ from nonlinear simulations.

In other contexts (Craik 1985; Bourlioux & Majda 1995), amplitude equations are derived by first assuming a leading-order solution with contributions from both eastward- and westward-propagating waves:

$$\alpha_+(\epsilon^2 t)\boldsymbol{e}_+(k)\mathrm{e}^{\mathrm{i}[kx-\omega_+(k)t]} + \alpha_-(\epsilon^2 t)\boldsymbol{e}_-(k)\mathrm{e}^{\mathrm{i}[kx-\omega_-(k)t]} + \text{c.c.} \tag{2.3}$$

where $T = \epsilon^2 t$ is a slow time scale, $\alpha_\pm(T)$ are complex-valued amplitudes, $\boldsymbol{e}_\pm(k)$ are the eigenvectors of the wavenumber-k linear modes, $\omega_\pm(k)$ are the frequencies of the wavenumber-k linear modes, and "c.c." stands for the complex conjugate. The systematic asymptotic procedure in other similar contexts would then yield coupled ODEs for the complex amplitudes:

$$\begin{aligned}\frac{\mathrm{d}\alpha_+}{\mathrm{d}T} &= \chi\alpha_+ + \beta|\alpha_+|^2\alpha_+ + \eta|\alpha_-|^2\alpha_+ \\ \frac{\mathrm{d}\alpha_-}{\mathrm{d}T} &= \chi\alpha_- + \beta|\alpha_-|^2\alpha_- + \eta|\alpha_+|^2\alpha_-\end{aligned} \tag{2.4}$$

From this it can be seen that the real-valued magnitudes $a_\pm(T) = |\alpha_\pm(T)|$ evolve according to

$$\begin{aligned}\frac{\mathrm{d}a_+}{\mathrm{d}T} &= \Gamma a_+ - d a_+^3 - s a_-^2 a_+ \\ \frac{\mathrm{d}a_-}{\mathrm{d}T} &= \Gamma a_- - d a_-^3 - s a_+^2 a_-\end{aligned} \tag{2.5}$$

where the variables $a_\pm(T)$ and the parameters Γ, d, b are all real-valued, and the parameters are determined in terms of the parameters of the original PDE for the nonlinear waves. In this model, the positive parameter $\Gamma > 0$ is the coefficient of the linear growth term, the positive parameter $d > 0$ is the coefficient of the nonlinear damping term, and the positive parameter $s > 0$ is the coefficient of the nonlinear interaction term between the two waves. [The parameter $b = -s$ was allowed to be either positive or negative in Bourlioux & Majda (1995), but we restrict to $s > 0$ here for simplicity.]

The competition between traveling and standing waves can be addressed in (2.5) through the stability of the corresponding fixed points. The nontrivial fixed points are the

(a) Traveling wave (eastward-propagating),

$$(a_+, a_-) = \left(\sqrt{\frac{\Gamma}{d}}\ ,\ 0 \right) \tag{2.6}$$

(b) Traveling wave (westward-propagating),

$$(a_+, a_-) = \left(0\ ,\ \sqrt{\frac{\Gamma}{d}} \right) \tag{2.7}$$

(c) Standing wave,

$$(a_+, a_-) = \left(\sqrt{\frac{\Gamma}{d+s}}\ ,\ \sqrt{\frac{\Gamma}{d+s}} \right). \tag{2.8}$$

The stability of these fixed points is determined by the values of the parameters d and s; a brief summary of Bourlioux & Majda (1995) is:

$$\begin{array}{lcl} d < s & : & \text{traveling wave is stable} \quad \text{and} \quad \text{standing wave is unstable} \\ s < d & : & \text{traveling wave is unstable} \quad \text{and} \quad \text{standing wave is stable} \end{array} \tag{2.9}$$

Parameter	Value
Γ	1.05×10^{-5} s^{-1}
d	1.11×10^{-7} s m^{-2}
s	9.50×10^{-8} s m^{-2}
	1.11×10^{-7} s m^{-2}
	1.27×10^{-7} s m^{-2}
C	1.47×10^{-8} m^{-1}
γ	1.00×10^{-6} m^{-1}

TABLE 1. Parameters for the amplitude models (2.5), (2.22), and (2.25).

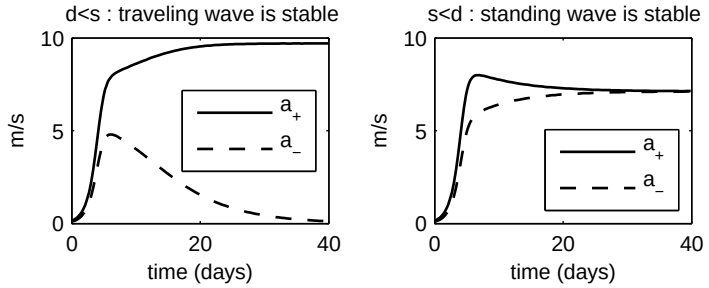

FIGURE 4. Dynamics of the amplitude model (2.5) for two parameter regimes. Left: Traveling wave is stable for $d < s$ (compare with left column of multicloud model simulations in figure 3). Right: Standing wave is stable for $s < d$ (compare with right column of multicloud model simulations in figure 3).

Figure 4 illustrates the solution to (2.5) for each of these parameter regimes. These different cases are comparable to the multicloud model results in figure 3, and they suggest that the background shear plays the role of the parameters d and s. The parameter values are listed in table 1; Γ was determined from the linear theory growth rate in figure 3, and d and s were chosen so that the fixed point amplitudes in (2.9) are comparable to the multicloud model results in figure 3. The amplitudes $a_\pm$ will be given velocity units throughout the paper to facilitate comparison with the mean flow amplitude.

In nature, one can think of the traveling wave state as a case where a single wave type is present in some region, and the standing wave state as a case where there is a mixture of different wave types present in some region. The competition between the two states is important for many reasons, such as energy exchanges between scales: a coherent wave can be expected to transport momentum to larger scales, whereas a mixture of wave types would not (due to cancellation of the different waves' momentum transports). This topic is investigated next.

2.2. *Effect of CCW on mean flow*

In the previous subsection, models were presented for the effect of a mean flow on CCW; in this subsection, the converse effect – the effect of the CCW on the mean flow – is considered using three models. First, an exactly solvable model is used to show when and how a CCW will affect the mean flow. Second, it is shown that the CCW from the PDE model in figure 3 should affect the mean flow. Third, an ODE model is presented that includes the effect of CCW on the mean flow.

First consider the following exactly solvable model for a CCW:

$$\begin{aligned} w'(x,z,t) &= S'_\theta(x,z,t) \\ \partial_x u' + \partial_z w' &= 0. \end{aligned} \tag{2.10}$$

In this model, called the weak-temperature-gradient approximation, the wave's vertical velocity w' is exactly in balance with the heating rate S'_θ, which we must specify. The wave's horizontal velocity u' is then determined from the incompressibility constraint in (2.10) (Majda & Biello 2004; Biello & Majda 2005). Given this exact solution for u' and w' of the CCW, its effect on the mean flow is determined by

$$\partial_t \bar{u} = -\partial_z \overline{w'u'}, \tag{2.11}$$

where this is the horizontal spatial average of the horizontal momentum equation, $\partial_t u + \partial_x(u^2) + \partial_z(wu) + \partial_x p = 0$, and where bar and prime notation is used to denote a horizontal spatial average and fluctuation, respectively:

$$\begin{aligned} \bar{f}(z,t) &= \frac{1}{L}\int_0^L f(x,z,t)\,\mathrm{d}x \\ f'(x,z,t) &= f - \bar{f}, \end{aligned} \tag{2.12}$$

where periodic horizontal boundary conditions are assumed for simplicity. From (2.11) it is seen that a CCW will alter the mean flow if and only if $\partial_z \overline{w'u'} \neq 0$. In the context of convective motions, this effect on the mean flow is called CMT.

To illustrate CMT in some specific cases, consider a heat source with two phase-lagged vertical modes, $\sin(z)$ and $\sin(2z)$, which represent deep convective heating and congestus/stratiform heating, respectively:

$$S'_\theta = a_* \left\{ \cos[kx - \omega t]\,\sqrt{2}\sin(z) + \alpha \cos[k(x+x_0) - \omega t]\,\sqrt{2}\sin(2z) \right\}, \tag{2.13}$$

where k is the horizontal wavenumber and a_* is the amplitude of the heating. Two key parameters here are α, the relative strength of the second baroclinic heating, and x_0, the lag between the heating in the two vertical modes. Figure 5 shows three cases for the lag x_0: 0 (top), +500 km (middle), and −500 km (bottom) for a wave with wavelength 3000 km, heating amplitude $a_* = 4$ K/day, and relative stratiform heating of $\alpha = -1/4$. The lag determines the vertical tilt of the heating profile. Given this heating rate, the velocity can be found exactly from (2.10):

$$\begin{aligned} u'(x,z,t) &= -\frac{a_*}{k}\left\{ \sin[kx - \omega t]\,\sqrt{2}\cos(z) + 2\alpha \sin[k(x+x_0) - \omega t]\,\sqrt{2}\cos(2z) \right\} \\ w'(x,z,t) &= a_* \left\{ \cos[kx - \omega t]\,\sqrt{2}\sin(z) + \alpha \cos[k(x+x_0) - \omega t]\,\sqrt{2}\sin(2z) \right\} \end{aligned} \tag{2.14}$$

With this form of u' and w', the eddy flux divergence is

$$\partial_z \overline{w'u'} = \frac{3}{2}\frac{\sin(kx_0)}{k}\, a_*^2\, \alpha[\cos(z) - \cos(3z)] \tag{2.15}$$

Notice that a wave with first and second baroclinic components generates CMT that affects the first and *third* baroclinic modes (Majda & Biello 2004; Biello & Majda 2005). The third baroclinic mode was not included in the earliest work with the multicloud model, and a third baroclinic wave momentum $u'_3(x,t)$ for the fluctuations is still not included here. However, a third baroclinic mode mean flow, $\bar{U}_3(T)$, is included in Majda & Stechmann (2009*a*) and here in order to capture the large scale effect of CMT; it will play an important role in the CCW–mean flow dynamics. Also notice that (2.15) is nonzero

as long as $\alpha \neq 0$ (i.e., there are both first and second baroclinic mode contributions) and $x_0 \neq 0$ (i.e., there is a phase lag between the first and second baroclinic modes). The CCWs in the multi-cloud model typically have this structure (Khouider & Majda 2006, 2008), in agreement with observed CCW (Kiladis *et al.* 2009).

For illustrations of the above exact solutions, consider the three cases shown in figure 5: upright updraft (top), "westward-propagating" CCW (middle), and "eastward-propagating" CCW (bottom). Although there is no inherent definitive propagation in the exactly solvable model (2.10), propagation direction labels are assigned to the vertical tilt directions according to the structures of observed CCW (Kiladis *et al.* 2009): heating is vertically tilted with leading low-level heating and trailing upper-level heating with respect to the CCW propagation direction. Also shown in figure 5 are the average vertical flux of horizontal momentum, $\overline{w'u'}$, and its vertical derivative, $\partial_z \overline{w'u'}$. These exact solutions show that upright updrafts have zero CMT, and tilted updrafts have nonzero CMT with the sign determined by the CCW's propagation direction.

Second, rather than the exactly solvable model, consider the velocity fluctuations u' and w' in figure 6 from the multicloud model, which are taken from the first case from figure 3 at time $t = 30$ days. The CCW has a vertically tilted updraft due to a heating structure from a combination of deep convection and stratiform heating. There is a positive momentum flux $\overline{w'u'}$ in the middle troposphere, which corresponds to a $-\partial_z \overline{w'u'}$ structure that would accelerate easterlies in the lower troposphere and westerlies in the upper troposphere, if this CMT were not balanced by other momentum sources. (In the next section, the mean wind will be allowed to evolve in response to this type of CMT.) Also note that the middle case from figure 3 also has a CCW structure as in figure 6, which, in that case, would decelerate the mean flow at all levels if the CMT were not balanced by other momentum sources. Together, these two cases illustrate that the energy transer can be either upscale or downscale, depending on the particular mean flow and the propagation direction of the CCW.

Third and finally, we describe a simple ODE model for the effect of CCW amplitudes, a_+ and a_-, on the mean flow. Recall the formula from (2.15) for the eddy flux divergence $\partial_z \overline{w'u'}$. Since its vertical structure is $\cos(z) - \cos(3z)$, only the $\bar{u}_1$ and $\bar{u}_3$ modes of $\bar{u}$ will be affected. In fact, only the $\bar{u}_1 - \bar{u}_3$ component will be affected; the $\bar{u}_1 + \bar{u}_3$ component will remain unchanged. For this reason, we define the dynamical part of the mean flow to be

$$U(T) = \bar{u}_1(T) - \bar{u}_3(T). \tag{2.16}$$

(Note the lack of an overbar to distinguish this from the vertical profile of the mean flow, $\bar{U}(z)$.) The effect of a CCW amplitude, a_+ or a_-, on the mean flow $U(T)$ can then be ascertained from (2.11) and (2.15). First, notice that the eddy flux divergence in (2.15) is proportional to a_*^2, i.e., quadratic in its dependence on the wave amplitude. Second, notice that it changes sign if the lag (and hence the tilt and propagation direction) changes sign. A simple model for these effects would then take the form

$$\frac{\mathrm{d}U}{\mathrm{d}T} = C(a_+^2 - a_-^2), \tag{2.17}$$

where C is a constant of proportionality and a_+ and a_- are the amplitudes of the eastward- and westward-propagating waves, as in (2.5). The value of C used here is shown in table 1; it can be estimated a priori using the model in (2.15) or checked a posteriori through the model comparisons in the next subsection.

The simple model (2.17) shows an important difference between the standing wave state with $a_+ = a_-$ and the traveling wave state with either $a_+ = 0$ or $a_- = 0$: a

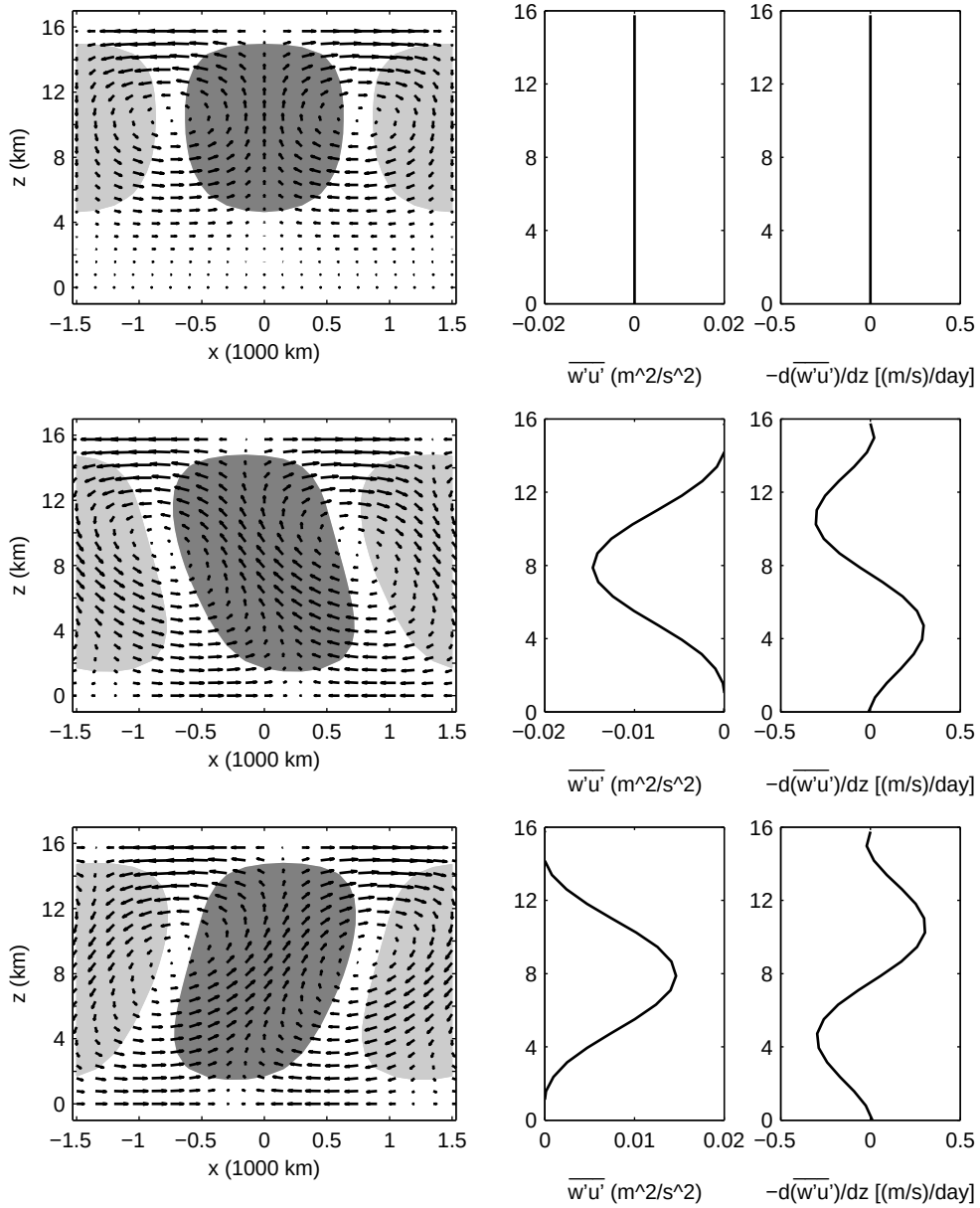

FIGURE 5. Solutions to the exactly solvable model (2.10) for CCW structure and CMT in three cases: upright updraft (top), vertically tilted updraft of "eastward-propagating" CCW (middle), and vertically tilted updraft of "westward-propagating" CCW (bottom). Left: Vector plot of (u', w') and shaded convective heating $S'_\theta(x, z)$. For vectors, the maximum u' is 6.0 m/s for the top and 4.0 m/s for the middle and bottom, and the maximum w' is 2.8 cm/s for the top and 2.2 cm/s for the middle and bottom. Dark shading denotes heating, and light shading denotes cooling, with a contour drawn at one-fourth the max and min values. Middle: Vertical profile of the mean momentum flux: $\overline{w'u'}$. Right: Negative vertical derivative of the mean momentum flux: $-\partial_z \overline{w'u'}$.

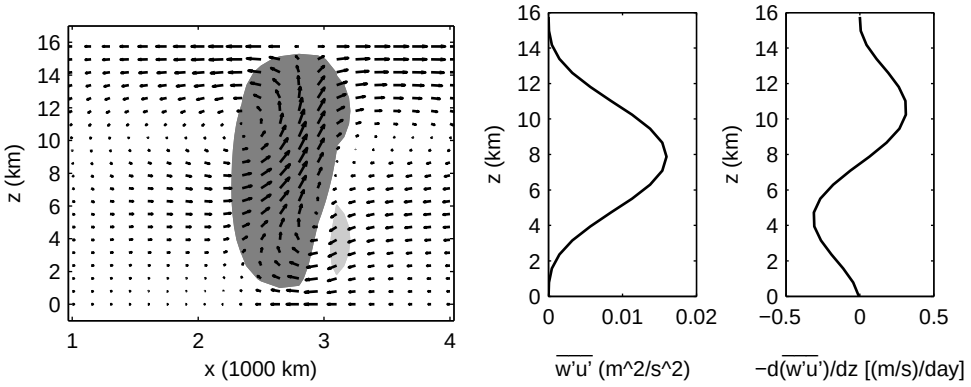

FIGURE 6. Structure and CMT of the westward-propagating CCW from the left case of figure 3 at time $t = 30$ days. Left: Vector plot of (u, w) and shaded convective heating. Maximum u and w are 5.2 m/s and 7.3 cm/s, respectively, and dark and light shading show convective heating greater than +2 K/day and less than -2 K/day, respectively. Middle: Vertical profile of the mean momentum flux: $\overline{w'u'}$. Right: Negative vertical derivative of the mean momentum flux: $-\partial_z \overline{w'u'}$.

standing wave state will not cause changes in the mean flow, whereas a traveling wave does change the mean flow.

2.3. *CCW–mean flow interactions*

Now the one-way effects of subsections 2.1 and 2.2 will be combined to allow two-way CCW–mean flow interactions. As before, both the multicloud model (2.1) and amplitude equations will be used.

To obtain CCW–mean flow interactions with the multicloud model, one key is to include a third baroclinic mode background wind $\bar{U}_3(T)$ that evolves on a long time scale $T = \epsilon^2 t$. Another key is to free the domain-mean wind from the parameterized momentum damping, $-u/\tau_u$, and instead to allow it to evolve according to the resolved CMT, $-\partial_z \langle \overline{w'u'} \rangle$, where $\langle f \rangle$ is the time average of f over the fast wave time scale. The practical details involved in implementing these changes with the multicloud model are explained in Majda & Stechmann (2009*a*) and are not repeated here. Instead, to give the idea of the multiscale model without the encumberance of the practical details, the theoretical multiscale asymptotic derivation from Majda & Stechmann (2009*a*) will be outlined.

A multiscale asymptotic model for CCW–environment interactions can be derived from the atmospheric primitive equations, as described by Majda & Stechmann (2009*a*). The derivation is outlined here for the zonal velocity u only, although the full set of atmospheric variables is used by Majda & Stechmann (2009*a*). The starting point is the two dimensional equation,

$$\partial_t u + \partial_x(u^2) + \partial_z(wu) + \partial_x p = S_u \tag{2.18}$$

It is assumed that the velocity depends on two time scales: a fast time scale t on equatorial synoptic scales, and a slow time scale $T = \epsilon^2 t$ on intraseasonal time scales. The asymptotic expansion of u takes the form

$$u = \bar{U}(z, T) + \epsilon u'(x, z, t, T) + \epsilon^2 u_2 + O(\epsilon^3) \tag{2.19}$$

with similar expansions for other variables, and where $\bar{U}(z, T)$ is the slowly varying mean wind and $u'(x, z, t, T)$ is the fluctuating wind. After inserting the ansatz (2.19)

into the primitive equation (2.18) and applying the procedure of systematic multiscale asymptotics, the result is

$$\begin{aligned} \partial_T \bar{U} &= -\partial_z \langle \overline{w'u'} \rangle \\ \partial_T \bar{\Theta} &= -\partial_z \langle \overline{w'\theta'} \rangle + \langle \overline{S_{\theta,2}} \rangle \\ \partial_z \bar{P} &= \bar{\Theta} \end{aligned} \tag{2.20}$$

and a set of equations for the fluctuations,

$$\begin{aligned} \partial_t u' + \bar{U}\partial_x u' + w'\partial_z \bar{U} + \partial_x p' &= S'_{u,1} \\ \partial_t \theta' + \bar{U}\partial_x \theta' + w'\partial_z \bar{\Theta} + w' &= S'_{\theta,1} \\ \partial_z p' &= \theta' \\ \partial_x u' + \partial_z w' &= 0 \end{aligned} \tag{2.21}$$

where the full derivation by Majda & Stechmann (2009*a*) includes the full set of atmospheric variables. The multiscale equations (2.20)–(2.21) demonstrate the main two mechanisms of CCW–mean flow interactions: CMT from the CCW drives changes in the mean wind on the slow time scale $T = \epsilon^2 t$, and the mean flow affects the CCW through the advection terms. By themselves, (2.20)–(2.21) include the dry dynamical basis and the multiscale interactions, but the source term $S'_{\theta,1}$ still needs to be specified; the multicloud model is thus used to supply interactive source terms and moisture effects. Note that (2.20)–(2.21) allows for changes in the mean thermodynamic state such as $\bar{\Theta}(z,T)$ in addition to mean flow $\bar{U}(z,T)$; this was also included in Majda & Stechmann (2009*a*) and here as well, but only the mean flow $\bar{U}(z,T)$ dynamics will be shown here as it has the most significant effect in this single-planetary-scale-column setup.

In short, the model for CCW–environment interactions can be thought of as the multiscale model in (2.20)–(2.21) with the multicloud model used to supply moisture effects and interactive source terms for (2.21). Figure 7 shows three cases from Majda & Stechmann (2009*a*) with the CCW evolution shown as well. These cases have an initial mid-tropospheric jet of different strength. For the left case with weaker climatological jet, CCW–mean flow oscillations arise on the long time scale. As part of this oscillation, the mean flow jet oscillates between the lower-middle troposphere and the upper-middle troposphere, and, simultaneously, the CCW grow, decay, and change their propagation direction. The evolution through one period from roughly time 500 to 600 days is as follows. At time 500 days, the mean flow has an upper-middle tropospheric jet, and the westward-propagating CCW is favored in the sense that its linear theory growth rate is larger than the eastward-propagating CCW's (not shown). From time 510 to 550 days, the CMT from this westward-propagating CCW then drives the jet to the lower-middle tropospere, and in this shear it is the eastward-propagating CCW that is favored. Hence, around time 550 days, the westward-propagating CCW decays, the eastward-propagating CCW amplifies, and the cycle repeats. In short, each CCW essentially creates its own demise. Also note that the CMT energy transfers in this case are both upscale and downscale: the jet is decelerated at one altitude and accelerated at a different altitude.

Figure 7 also shows a Hopf bifurcation: the stable fixed point becomes unstable and locks into an irregular limit cycle as the climatological jet strength is decreased. The stable fixed point corresponds to a fixed mean jet and a CCW standing oscillation. In the middle case, at the point of neutral stability, the mean jet has small oscillations, and the CCWs both have nontrivial amplitudes that also have small oscillations on the long time scale. The period of the small amplitude oscillations is shorter than the large-amplitude oscillations in the left case.

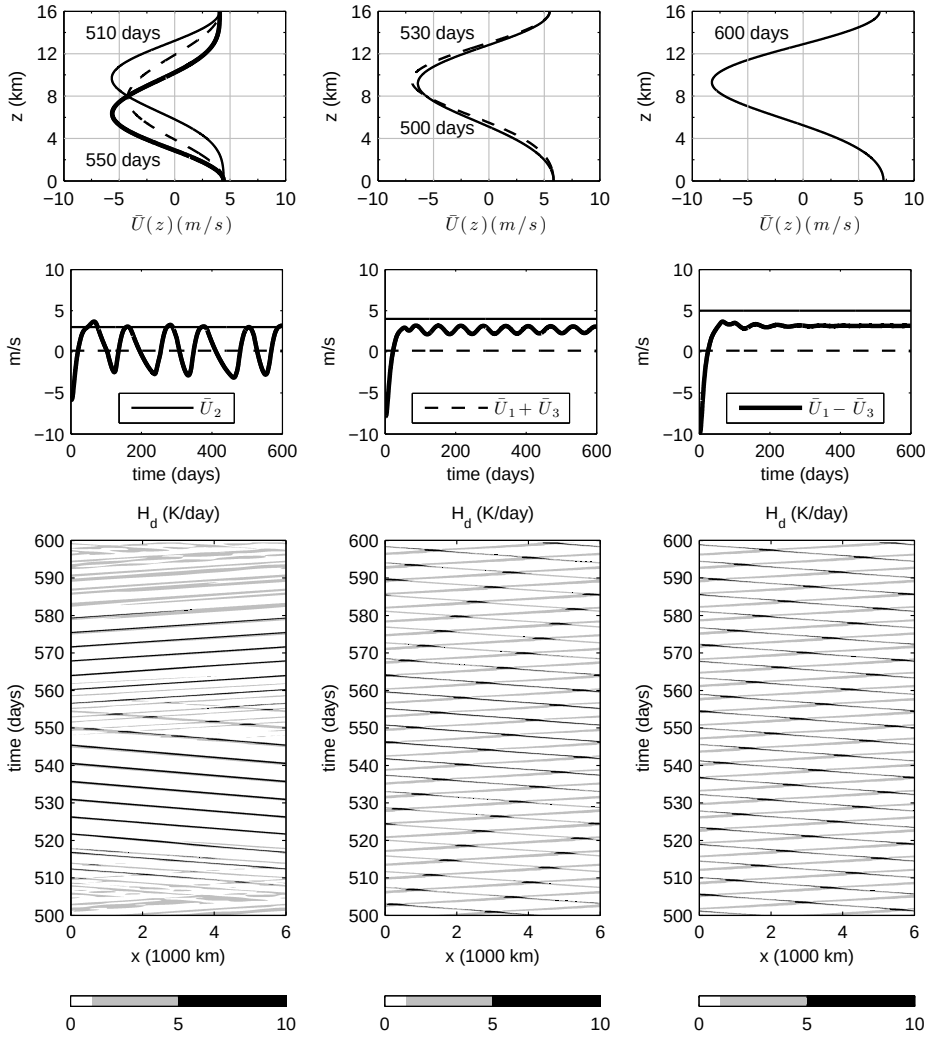

FIGURE 7. Nonlinear simulations with the multiscale multicloud model for three climatological background shears: weaker (left), intermediate (middle), and stronger (right). Row 1: Snapshots of mean wind $\bar{U}(z,T)$ at different times. Row 2: Evolution in time of the mean wind vertical modes from time 0 to 600 days: $\bar{U}_2$ (thin solid), $\bar{U}_1+\bar{U}_3$ (thin dashed), and $\bar{U}_1-\bar{U}_3$ (thick solid). Row 3: Space–time plots of deep convective heating $H_d(x,t)$ of the CCW from time 500 to 600 days.

For a simplified ODE model of the CCW–mean flow interactions, the amplitude models (2.5) and (2.17) can be combined to give the **CCW–mean flow amplitude ODEs**:

$$\begin{aligned}
\frac{\mathrm{d}U}{\mathrm{d}T} &= C(a_+^2 - a_-^2), \\
\frac{\mathrm{d}a_+}{\mathrm{d}T} &= (\Gamma - \gamma U)a_+ - da_+^3 - sa_-^2 a_+ \\
\frac{\mathrm{d}a_-}{\mathrm{d}T} &= (\Gamma + \gamma U)a_- - da_-^3 - sa_+^2 a_-
\end{aligned} \tag{2.22}$$

Additional terms $\mp\gamma U a_\pm$ were added to these equations to account for the effect of mean flow changes on the CCW growth rates. The linear dependence $\Gamma \pm \gamma U$ of the growth rate

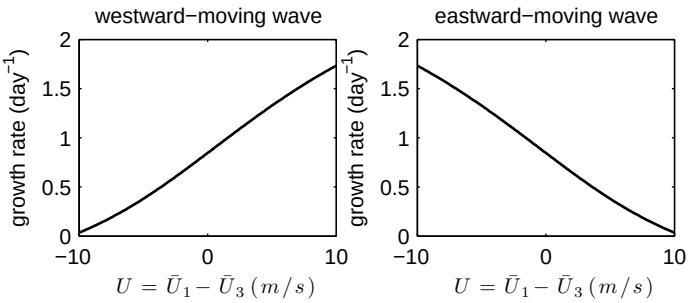

FIGURE 8. Maximum linear theory growth rate of the multicloud model as a function of $\bar{U}_1 - \bar{U}_3$ for the westward-propagating unstable mode (left) and the eastward-propagating unstable mode (right).

on U is shown to be a good fit based on linear theory with the multicloud model, shown in figure 8, and it provides an estimated parameter value of $\gamma = 0.086$ day^{-1} (m/s)$^{-1}$. Also note that this real-valued cubic nonlinear system could be reduced to a quadratically nonlinear system by changing variables from $a_\pm$ to $a_\pm^2$, but we do not employ this change here.

The amplitude model in (2.22) has a standing wave fixed point given by

$$(U, a_+, a_-) = \left(0\ ,\ \sqrt{\frac{\Gamma}{d+s}}\ ,\ \sqrt{\frac{\Gamma}{d+s}} \right). \tag{2.23}$$

but it does not have a traveling wave fixed point, due to the mean flow dynamics. The linear stability of this fixed point shows the same parameter dependence as the amplitude model (2.9):

$$\begin{array}{rcl} d < s & : & \text{standing wave is unstable} \\ s < d & : & \text{standing wave is stable} \end{array} \tag{2.24}$$

Figure 9 shows numerical solutions of the amplitude model (2.22) for three parameter regimes: $d < s$ (left), $s = d$ (middle), and $s < d$ (right), using the values from table 1. In combination with the linear stability analysis (2.24), these numerical results demonstrate a Hopf bifurcation: as the parameter s is increased from $s < d$ to $d < s$, the standing wave fixed point becomes unstable and a stable limit cycle appears. Moreover, these three cases are comparable to the multicloud model results seen in figure 7. The oscillatory case on the left even captures the ramp–step-like dynamics of the wave amplitude, where long periods of time with only one significant wave amplitude are punctuated by somewhat rapid transitions between wave amplitudes. However, the transitions between a_+ and a_- occur more rapidly than they do for the spatially resolved CCW in figure 7, and this leads to a sawtooth-like evolution in $U(T)$. In the middle case, there is initially a sawtooth-like dynamics, but it slowly evolves into a smaller-amplitude shorter-period oscillation that is more sinusoidal. Eventually the dynamics locks into a regular small-amplitude oscillation with period of roughly 45 days and with $U(T)$ taking values 6.5 ± 1.5 m/s and $a_\pm$ taking values 0 ± 0.3 m/s (not shown).

For the oscillator cases, an even simpler amplitude model with the basic mechanism of the CCW–mean flow oscillations is

$$\frac{\mathrm{d}U}{\mathrm{d}T} = C(a_+^2 - a_-^2)$$
$$\frac{\mathrm{d}a_+}{\mathrm{d}T} = -\gamma U a_+$$

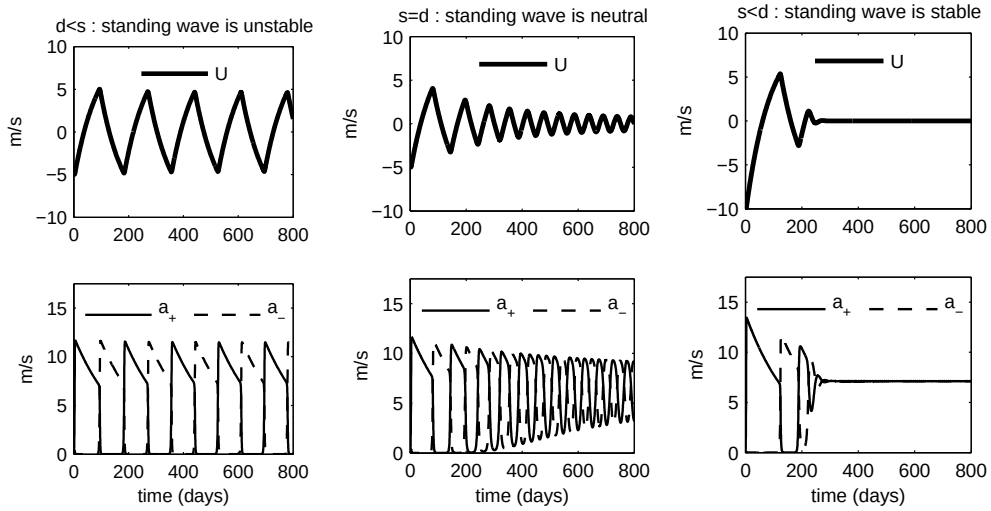

FIGURE 9. Numerical solution to amplitude model (2.22) for CCW–mean flow interaction for three parameter regimes: $d < s$ (left), $s = d$ (middle), and $s < d$ (right). Compare with three multicloud model simulations in figure 7, respectively. Top row: Mean wind amplitude, $U(T)$. Bottom row: CCW amplitudes, $a_+(T)$ (solid) and $a_-(T)$ (dashed).

$$\frac{\mathrm{d}a_-}{\mathrm{d}T} = +\gamma U a_- \tag{2.25}$$

which is the same as (2.22) except the cubic terms and the linear growth terms have been left out. Figure 10 shows numerical solutions for two cases: large-amplitude oscillations (left) and small-amplitude oscillations (right). These are meant for comparison with the first two cases in figure 9 for (2.22) and in figure 7 for the multicloud model. The simple model (2.25) captures the basic oscillatory behavior, including the longer oscillation period corresponding to larger-amplitude oscillations. While there are several similarities, many details of the large-amplitude oscillations are different from (2.22). For example, (2.25) misses the ramp–step-like behavior of the CCW amplitude seen in figures 7 and 9, but it includes periods of time when the mean flow $U(T)$ is essentially unchanging, due to weak convective momentum transports; this latter behavior is actually seen to a small extent in the first case in figure 7 and to a large extent in other cases shown by Majda & Stechmann (2009*a*) (see their figures 6 and 7). Another property of (2.25) is that it is a neutrally stable model, and hence its initial conditions determine the oscillation amplitude to a large degree. In fact, (2.25) has two conserved quantities

$$E = \gamma U^2 + C(a_+^2 + a_-^2), \qquad \text{and} \qquad A = a_+ a_-, \tag{2.26}$$

which represent a sort of energy and a product of CCW amplitudes. Furthermore, (2.25) is actually equivalent to Duffing's equation, as it can be rewritten as

$$\frac{\mathrm{d}^2 U}{\mathrm{d}T^2} = -2\gamma U(E - \gamma U^2) \tag{2.27}$$

3. CCW-water vapor interactions: the MJO skeleton

In the tropical troposphere, it is not only CCW–mean flow interactions that are important but also CCW–water vapor interactions. In fact, Majda & Stechmann (2009*b*)

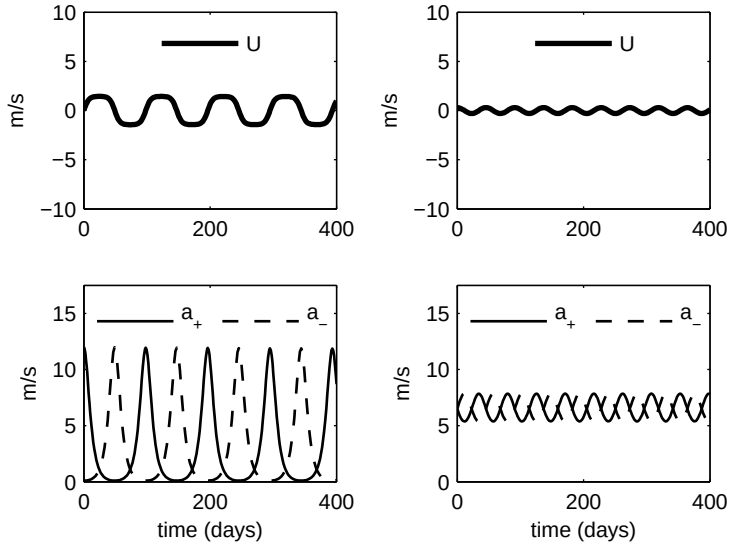

FIGURE 10. Numerical solution to the simple oscillatory amplitude model (2.25) for CCW–mean flow interaction for large-amplitude oscillations (left) and small-amplitude oscillations (right). Compare with the first two cases in figure 9 for the cubic nonlinear amplitude model (2.22) (and note the difference in plotted time interval). Top row: Mean wind amplitude, $U(T)$. Bottom row: CCW amplitudes, $a_+(T)$ (solid) and $a_-(T)$ (dashed).

proposed a minimal model for the skeleton of the MJO and tropical intraseasonal variability, and the proposed fundamental mechanism is CCW–water vapor interactions, coupled with planetary-scale fluid dynamics. The model includes an amplitude equation in the spirit of (2.25), coupled with the linearized (long-wave-scaled) moist primitive equations:

$$\partial_T a = \gamma_q q a \tag{3.1}$$

$$\partial_T q - \tilde{Q} w = -\bar{H} a + S^q \tag{3.2}$$

$$\partial_T \theta + w = \bar{H} a - S^\theta \tag{3.3}$$

$$\partial_T u - y v = -\partial_X p \tag{3.4}$$

$$y u = -\partial_y p \tag{3.5}$$

$$0 = -\partial_z p + \theta \tag{3.6}$$

$$\partial_X u + \partial_y v + \partial_z w = 0 \tag{3.7}$$

The amplitude dynamics in (3.1) arises from

$$\frac{\mathrm{d}a_\pm}{\mathrm{d}T} = \gamma_q q a_\pm \qquad \text{and} \qquad a(T) = a_+(T) + a_-(T) \tag{3.8}$$

where it is only the total amplitude $a(t)$ that is important in this context of water vapor interactions, not the detailed competition between the different wave types a_+ and a_-. Furthermore, in nature, there would actually be not only the two convectively coupled gravity wave types a_+ and a_- but the complex menagerie of equatorial shallow water waves coupled with convection, including Kelvin waves, mixed Rossby–gravity waves, etc. (Majda 2003; Kiladis *et al.* 2009).

The important parameter γ_q in (3.1) can be estimated theoretically from the multicloud model, as was also the case for the amplitude model parameters from section 2. The parameter γ_q represents the change in the CCW growth rate per unit change in

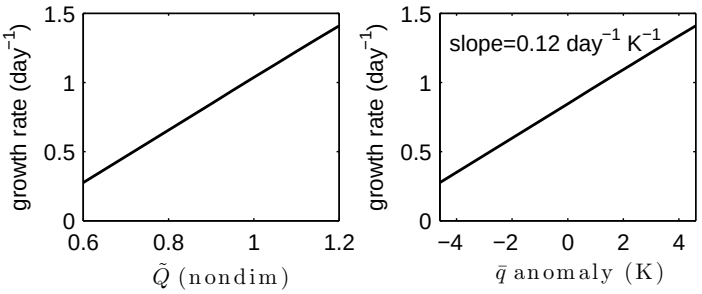

FIGURE 11. Maximum linear theory growth rate of the multicloud model as a function of the nondimensional parameter $\tilde{Q}$ (left) and translated to anomalous dimensional units (right). The curve is approximately linear with a slope of roughly 0.12 day^{-1} K^{-1}.

background water vapor. The background water vapor enters into the multicloud model in several places that could potentially be complicated (Khouider & Majda 2006). The simplest place is in the water vapor equation

$$\partial_t q + \partial_x[q(u_1 + \tilde{\alpha}u_2)] + \tilde{Q}\partial_x(u_1 + \tilde{\lambda}u_2) = -P + \frac{1}{H_T}D \tag{3.9}$$

If q on the left hand side is split into background $\bar{q}$ and fluctuation q' contributions, then (3.9) becomes

$$\partial_t q' + \partial_x[q'(u_1 + \tilde{\alpha}u_2)] + \bar{q}\partial_x(u_1 + \tilde{\alpha}u_2) + \tilde{Q}\partial_x(u_1 + \tilde{\lambda}u_2) = -P + \frac{1}{H_T}D \tag{3.10}$$

From this it is seen that, to some degree, the background water vapor $\bar{q}$ has the same effect as the parameter $\tilde{Q}$. Figure 11 shows the maximum linear theory growth rate as a function of $\tilde{Q}$, centered on the standard nondimensional value $\tilde{Q} = 0.9$. The linear approximation $\Gamma + \gamma_q(\tilde{Q} - 0.9)$ is a good fit. After translating this result from nondimensional $\tilde{Q}$ to the background water vapor $\bar{q}$ in dimensional units, one finds an estimate of $\gamma_q \approx 0.12$ day^{-1} K^{-1}, which is in good agreement with the standard value of 0.19 day^{-1} K^{-1} conjectured by Majda & Stechmann (2009*b*). It would be interesting to try to estimate γ_q from observational analysis as well.

4. Concluding discussion

Two types of CCW–environment interactions were investigated – CCW–mean flow and CCW–water vapor interactions – and they were investigated with two types of models: the spatially varying multicloud model and amplitude ODEs. The basic mechanisms of the CCW–mean flow interactions are that (i) the mean flow's vertical shear determines the preferred propagation direction of the CCW, and (ii) the CCWs can drive changes in the mean flow through convective momentum transport, with energy transfer that is sometimes upscale and sometimes downscale. A multiscale version of the multicloud model showed CCW–mean flow interactions with nonlinear oscillations and a Hopf bifurcation as the climatological background wind is varied. These features were also captured by a set of amplitude ODEs, which were motivated by amplitude equations in other fluid dynamics settings. In the oscillatory regime, the amplitude equations displayed a ramp–step-like dynamics, in qualitative agreement with the multicloud model CCW dynamics. In addition, an even simpler amplitude model was also presented, and it was shown to be equivalent to the Duffing oscillator.

While the amplitude equations reproduced many of the features of the spatially varying model, it is also an idealized representation that has its limitations. For instance, using amplitude variables like $a_\pm$ does not account for the wide variety of spatial variability that is possible. While the cases shown here in figure 7 tend to show simple types of spatial variability with either a single westward- or eastward-propagating CCW present at each time, other cases shown in Majda & Stechmann (2009*a*) show finer-scale spatial variability that resembles the schematic picture in figure 1 and that has important consequences for CMT. When the finer scale fluctuations are present, the total CMT is often weaker, partly because the tilted updraft tends to be less coherent. Some of these consequences are studied further in the recent work of Khouider *et al.* (2011*a*), and they are likely not adequately represented by the amplitude ODEs studied here.

In the second part of this paper, CCW–water vapor interactions were investigated in the context of the MJO skeleton model of Majda & Stechmann (2009*b*, 2011). In that model, a simple amplitude equation is used to represent the dynamics of the planetary-scale envelope of sub-planetery-scale convection/wave activity. Here, the key parameter of that model is estimated theoretically using linear stability analysis of CCW in the multicloud model. The theoretical estimate is in agreement with previously conjectured values from Majda & Stechmann (2009*b*).

The results here demonstrate some of the interesting dynamics of wave–convection–environment interactions in the tropical troposphere. While the results presented were targeted at CCW specifically, many of the ideas here should also be relevant for other scales of the rich variety of tropical wave–convection–environment interactions, as described in the introduction section. Further studies – theoretical, numerical, and observational – are needed to gain a better understanding of the hierarchy of organized tropical convection.

The research of S. N. S. has been partially supported by a NOAA Climate and Global Change Postdoctoral Fellowship, a NSF Mathematical Sciences Postdoctoral Research Fellowship, and a start-up grant from the University of Wisconsin–Madison. The research of A. J. M. is partially supported by NFS grant DMS-0456713, NSF CMG grant DMS-1025468, and ONR grants ONR-DRI N00014-10-1-0554 and N00014-11-1-0306. D. S. was supported by the 2009 UCLA Applied Math REU through grant NSF DMS–0601395.

Appendix A. The Multicloud Model with Advection

The multicloud model with advection is the following set of seven equations:

$$\frac{\partial u_1}{\partial t} - \frac{\partial \theta_1}{\partial x} = -\frac{1}{\tau_u}(u_1 - \bar{U}_1) - \frac{1}{2\sqrt{2}}\left[6u_2\frac{\partial u_1}{\partial x} + (3u_1 + 5\bar{U}_3)\frac{\partial u_2}{\partial x}\right] \tag{A 1}$$

$$\frac{\partial u_2}{\partial t} - \frac{\partial \theta_2}{\partial x} = -\frac{1}{\tau_u}(u_2 - \bar{U}_2) - 2\sqrt{2}\bar{U}_3\frac{\partial u_1}{\partial x} \tag{A 2}$$

$$\begin{aligned}\frac{\partial \theta_1}{\partial t} - \frac{\partial u_1}{\partial x} &= H_d + \xi_s H_s + \xi_c H_c - R_1 \\ &\quad - \frac{1}{2\sqrt{2}}\left[-2u_2\frac{\partial \theta_1}{\partial x} + 4(u_1 - \bar{U}_3)\frac{\partial \theta_2}{\partial x} + 8\theta_2\frac{\partial u_1}{\partial x} - (\theta_1 - 9\bar{\Theta}_3)\frac{\partial u_2}{\partial x}\right]\end{aligned} \tag{A 3}$$

$$\begin{aligned}\frac{\partial \theta_2}{\partial t} - \frac{1}{4}\frac{\partial u_2}{\partial x} &= H_c - H_s - R_2 \\ &\quad + \frac{1}{2\sqrt{2}}\left[-(u_1 - \bar{U}_3)\frac{\partial \theta_1}{\partial x} + (\theta_1 - 9\bar{\Theta}_3)\frac{\partial u_1}{\partial x} - 8\bar{\Theta}_4\frac{\partial u_2}{\partial x}\right]\end{aligned} \tag{A 4}$$

$$\frac{\partial \theta_{eb}}{\partial t} = \frac{1}{h_b}(E - D) + \frac{1}{\pi}\frac{H_T}{h_b}\left[4\theta_2 \frac{\partial u_1}{\partial x} + \theta_1 \frac{\partial u_2}{\partial x}\right] \tag{A 5}$$

$$\frac{\partial q}{\partial t} + \tilde{Q}\frac{\partial}{\partial x}(u_1 + \tilde{\lambda} u_2) = -P + \frac{1}{H_T}D - \frac{\partial}{\partial x}[q(u_1 + \tilde{\alpha} u_2)] \tag{A 6}$$

$$\frac{\partial H_s}{\partial t} = \frac{1}{\tau_s}(\alpha_s P - H_s) + \left[A_s u_1 \frac{\partial H_s}{\partial x} + \frac{1}{2} A_s H_s \frac{\partial u_1}{\partial x}\right] \tag{A 7}$$

The variables u_j are the jth baroclinic mode velocity, θ_j are the jth baroclinic mode potential temperature, θ_{eb} is the boundary layer equivalent potential temperature, and q is the vertically integrated water vapor. Note that the nonlinear advection terms are written on the right hand side here. The source terms for these equations are

$$H_c = \alpha_c \frac{\Lambda - \Lambda^*}{1 - \Lambda^*} Q_c \tag{A 8}$$

$$H_d = \frac{1 - \Lambda}{1 - \Lambda^*} Q_d \tag{A 9}$$

$$P = \frac{2\sqrt{2}}{\pi}(H_d + \xi_s H_s + \xi_c H_c) \tag{A 10}$$

$$Q_d = \left[\bar{Q} + \frac{1}{\tau_{conv}}(a_1 \theta_{eb} + a_2 q - a_0(\theta_1 + \gamma_2 \theta_2 + \gamma_3 \bar{\Theta}_3 + \gamma_4 \bar{\Theta}_4))\right]^+ \tag{A 11}$$

$$Q_c = \left[\bar{Q} + \frac{1}{\tau_{conv}}(\theta_{eb} - a_0'(\theta_1 + \gamma_2' \theta_2 + \gamma_3' \bar{\Theta}_3 + \gamma_4' \bar{\Theta}_4))\right]^+ \tag{A 12}$$

$$\Lambda = \begin{cases} \Lambda^* & \text{for} \quad \theta_{eb} - \theta_{em} < \theta^- \\ \Lambda^* + (1 - \Lambda^*)\frac{\theta_{eb} - \theta_{em} - \theta^-}{\theta^+ - \theta^-} & \text{for} \quad \theta^- < \theta_{eb} - \theta_{em} < \theta^+ \\ 1 & \text{for} \quad \theta^+ < \theta_{eb} - \theta_{em} \end{cases} \tag{A 13}$$

$$\theta_{em} = q + \frac{2\sqrt{2}}{\pi}(\theta_1 + \alpha_2 \theta_2 + \alpha_3 \bar{\Theta}_3) \tag{A 14}$$

$$R_j = \frac{1}{\tau_\theta}\theta_j + Q_{R,j}^0, \qquad j = 1, 2 \tag{A 15}$$

$$\frac{1}{h_b}E = \frac{1}{\tau_e}(\theta_{eb}^* - \theta_{eb}) \tag{A 16}$$

$$D = \frac{m_0}{P_D}(P_D + \mu_2(H_s - H_c))^+(\theta_{eb} - \theta_{em}). \tag{A 17}$$

Notice that Λ in (A 13) is a nonlinear switch, and the superscript + in (A 11), (A 12), and (A 17) also represents a nonlinear switch, defined as $f^+ = \max(0, f)$ (although the superscript + of θ^+ in (A 13) does not take this meaning as θ^+ is just a constant parameter). The source terms H_c, H_d, and H_s represent heating from congestus, deep convective, and stratiform clouds, respectively. Radiative cooling is R_j, evaporation is E, downdrafts are D.

These are the equations of the multicloud model of Khouider & Majda (2008), with advection terms added using vertical mode projections as described by Stechmann *et al.* (2008), and with a few other changes described in Majda & Stechmann (2009*a*), where all parameter values are also described.

The linearized version of the multicloud model equations without background shear has been developed in mathematical detail elsewhere (Khouider & Majda 2006, 2008). It is straightforward to linearize the quadratic advection terms at a mean background

shear to produce the complete linearized equations that have been used throughout this paper for linear stability analysis.

REFERENCES

Andrews, D. G. & McIntyre, M. E. 1978 An exact theory of nonlinear waves on a Lagrangian-mean flow. *J. Fluid Mech.* **89** (4), 609–646.

Baldwin, M.P., Gray, L.J., Dunkerton, T.J., Hamilton, K., Haynes, P.H., Randel, W.J., Holton, J.R., Alexander, M.J., Hirota, I., Horinouchi, T., Jones, D.B.A., Kinnersly, J.S., Marquardt, C. andSato, K. & Takahashi, M. 2001 The quasi-biennial oscillation. *Rev. Geophys.* **39** (2), 179–229.

Barnes, G.M. & Sieckman, K. 1984 The environment of fast-and slow-moving tropical mesoscale convective cloud lines. *Monthly Weather Review* **112** (9), 1782–1794.

Benedict, J.J. & Randall, D.A. 2009 Structure of the Madden-Julian Oscillation in the Superparameterized CAM. *J. Atmos. Sci.* **66** (11), 3277–3296.

Biello, J. A. & Majda, A. J. 2005 A new multiscale model for the Madden–Julian oscillation. *J. Atmos. Sci.* **62**, 1694–1721.

Bourlioux, A. & Majda, A. J. 1995 Theoretical and numerical structure of unstable detonations. *Phil. Trans. Roy. Soc. London A* **350**, 29–68.

Bühler, O. 2009 *Waves and Mean Flows*. Cambridge University Press, Cambridge.

Craik, A. D. D. 1985 *Wave Interactions and Fluid Flows*. Cambridge Univ Press, Cambridge.

Dunkerton, T. J. & Crum, F. X. 1995 Eastward propagating ∼2- to 15-day equatorial convection and its relation to the tropical intraseasonal oscillation. *J. Geophys. Res.* **100** (D12), 25781–25790.

Grabowski, W. W. & Moncrieff, M. W. 2001 Large-scale organization of tropical convection in two-dimensional explicit numerical simulations. *Q. J. Roy. Met. Soc.* **127**, 445–468.

Guckenheimer, J. & Mahalov, A. 1992 Resonant triad interactions in symmetric systems. *Physica D: Nonlinear Phenomena* **54** (4), 267–310.

Hendon, H. H. & Liebmann, B. 1994 Organization of convection within the Madden–Julian oscillation. *J. Geophys. Res.* **99**, 8073–8084.

Houze, Jr., R. A. 1989 Observed structure of mesoscale convective systems and implications for large-scale heating. *Q. J. Roy. Met. Soc.* **115** (487), 425–461.

Houze, Jr., R. A. 2004 Mesoscale convective systems. *Rev. Geophys.* **42**, G4003+.

Johnson, R. H., Aves, S. L., Ciesielski, P. E. & Keenan, T. D. 2005 Organization of oceanic convection during the onset of the 1998 East Asian summer monsoon. *Mon. Wea. Rev.* **133** (1), 131–148.

Khouider, B., Han, Y., Majda, A. J. & Stechmann, S. N. 2011*a* Multi-scale waves in an MJO background and CMT feedback. *J. Atmos. Sci.* p. submitted.

Khouider, B. & Majda, A. J. 2006 A simple multicloud parameterization for convectively coupled tropical waves. Part I: Linear analysis. *J. Atmos. Sci.* **63**, 1308–1323.

Khouider, B. & Majda, A. J. 2008 Multicloud models for organized tropical convection: enhanced congestus heating. *J. Atmos. Sci.* **65**, 895–914.

Khouider, B., St-Cyr, A., Majda, A. J. & Tribbia, J. 2011*b* MJO and convectively coupled waves in a coarse resolution GCM with a simple multicloud parameterization. *J. Atmos. Sci.* p. in press.

Kiladis, G. N., Wheeler, M. C., Haertel, P. T., Straub, K. H. & Roundy, P. E. 2009 Convectively coupled equatorial waves. *Rev. Geophys.* **47**, RG2003.

Kim, D., Sperber, K., Stern, W., Waliser, D., Kang, I.-S., Maloney, E., Wang, W., Weickmann, K., Benedict, J., Khairoutdinov, M. *et al.* 2009 Application of MJO simulation diagnostics to climate models. *J. Climate* **22** (23), 6413–6436.

Lau, W. K. M. & Waliser, D. E., ed. 2005 *Intraseasonal Variability in the Atmosphere–Ocean Climate System*. Springer, Berlin.

LeMone, M.A. 1983 Momentum transport by a line of cumulonimbus. *J. Atmos. Sci.* **40** (7), 1815–1834.

LeMone, M.A. & Moncrieff, M.W. 1994 Momentum and mass transport by convective

bands: comparisons of highly idealized dynamical models to observations. *J. Atmos. Sci.* **51** (2), 281–305.

LeMone, M.A., Zipser, E.J. & Trier, S.B. 1998 The role of environmental shear and thermodynamic conditions in determining the structure and evolution of mesoscale convective systems during TOGA COARE. *J. Atmos. Sci.* **55** (23), 3493–3518.

Lin, J.-L., Kiladis, G. N., Mapes, B. E., Weickmann, K. M., Sperber, K. R, Lin, W., Wheeler, M., Schubert, S. D., Del Genio, A., Donner, L. J., Emori, S., Gueremy, J.-F., Hourdin, F., Rasch, P. J., Roeckner, E. & Scinocca, J. F. 2006 Tropical intraseasonal variability in 14 IPCC AR4 climate models Part I: Convective signals. *J. Climate* **19**, 2665–2690.

Majda, A. J. 2003 *Introduction to PDEs and Waves for the Atmosphere and Ocean*, *Courant Lecture Notes in Mathematics*, vol. 9. Providence: American Mathematical Society.

Majda, A. J. & Biello, J. A. 2004 A multiscale model for the intraseasonal oscillation. *Proc. Natl. Acad. Sci. USA* **101** (14), 4736–4741.

Majda, A. J. & Stechmann, S. N. 2009*a* A simple dynamical model with features of convective momentum transport. *J. Atmos. Sci.* **66**, 373–392.

Majda, A. J. & Stechmann, S. N. 2009*b* The skeleton of tropical intraseasonal oscillations. *Proc. Natl. Acad. Sci.* **106** (21), 8417.

Majda, A. J. & Stechmann, S. N. 2011 Nonlinear dynamics and regional variations in the MJO skeleton. *J. Atmos. Sci.* p. accepted.

Mapes, B. 1993 Gregarious tropical convection. *J. Atmos. Sci.* **50** (13), 2026–2037.

Moncrieff, M. W. & Green, J. S. A. 1972 The propagation and transfer properties of steady convective overturning in shear. *Q. J. Roy. Met. Soc.* **98** (416), 336–352.

Nakazawa, T. 1988 Tropical super clusters within intraseasonal variations over the western Pacific. *J. Met. Soc. Japan* **66** (6), 823–839.

Plumb, R. A. 1977 The interaction of two internal waves with the mean flow: Implications for the theory of the quasi-biennial oscillation. *J. Atmos. Sci.* **34**, 1847–1858.

Roundy, P.E. & Frank, W.M. 2004 A climatology of waves in the equatorial region. *J. Atmos. Sci.* **61** (17), 2105–2132.

Ruzmaikin, A., Lawrence, J. & Cadavid, C. 2003 A simple model of stratospheric dynamics including solar variability. *Journal of Climate* **16** (10), 1593–1600.

Stechmann, S. N. & Majda, A. J. 2009 Gravity waves in shear and implications for organized convection. *J. Atmos. Sci.* **66**, 2579–2599.

Stechmann, S. N., Majda, A. J. & Khouider, B. 2008 Nonlinear dynamics of hydrostatic internal gravity waves. *Theor. Comp. Fluid Dyn.* **22**, 407–432.

Takayabu, Y. N. 1994*a* Large-scale cloud disturbances associated with equatorial waves. I: Spectral features of the cloud disturbances. *J. Meteor. Soc. Japan* **72** (3), 433–449.

Takayabu, Y. N. 1994*b* Large-scale cloud disturbances associated with equatorial waves. II: Westward-propagating inertio-gravity waves. *J. Meteor. Soc. Japan* **72** (3), 451–465.

Tulich, S. N., Randall, D. & Mapes, B. 2007 Vertical-mode and cloud decomposition of large-scale convectively coupled gravity waves in a two-dimensional cloud-resolving model. *J. Atmos. Sci.* **64**, 1210–1229.

Wheeler, M. & Kiladis, G. N. 1999 Convectively coupled equatorial waves: analysis of clouds and temperature in the wavenumber–frequency domain. *J. Atmos. Sci.* **56** (3), 374–399.

Wheeler, M., Kiladis, G. N. & Webster, P. J. 2000 Large-scale dynamical fields associated with convectively coupled equatorial waves. *J. Atmos. Sci.* **57** (5), 613–640.

Yanai, M., Esbensen, S. & Chu, J. H. 1973 Determination of bulk properties of tropical cloud clusters from large-scale heat and moisture budgets. *J. Atmos. Sci.* **30**, 611–627.

Yang, G.Y., Hoskins, B. & Slingo, J. 2007 Convectively coupled equatorial waves. Part I: Horizontal and vertical structures. *J. Atmos. Sci.* **64** (10), 3406–3423.

Zhang, C. 2005 Madden–Julian Oscillation. *Reviews of Geophysics* **43**, G2003+.